Available online at www.elixirpublishers.com (Elixir International Journal)

Electrical Engineering

Elixir Elec. Engg. 116 (2018) 50050-50057

ISSN: 2229-712X

Carrier-Based Pulse Width Modulation Methods For B3-VSI Fed Induction Motor Drives

Imen Nouira El Badsi, Bassem El Badsi and Ahmed Masmoudi

Laboratory of Renewable Energies and Electric Vehicles, National, Engineering School of Sfax, P.O. Box 1173, 3038 Sfax.

ARTICLE INFO

Article history:

Received: 22 January 2018;
Received in revised form:
27 February 2018;
Accepted: 9 March 2018;

Keywords

Delta inverter,
Induction Motor,
Carrier-Based PWM Methods,
Simulation,
Experimental Results.

ABSTRACT

This paper investigates a comparative evaluation of carrier-based pulsewidth modulation (CB-PWM) methods devoted to the control of a B3-VSI, also known delta inverter, feeding an open-loop induction motor (IM) drives. Four CB-PWM methods namely: (i) sinusoidal PWM (SPWM), (ii) third-harmonic injection PWM (THI-PWM), (iii) optimal PWM (OPT-PWM), and (iv) space-vector PWM (SV-PWM) are analytically presented in order to control a delta inverter. The performance of the CB-PWM methods under consideration are firstly presented and therefore their control performances are analyzed and compared based on simulation and experimental results. The comparison is achieved by an investigation of the total and partial harmonic distortion ratios of the IM stator phase current.

1. Introduction

Dealing with three-switch inverters, two main classes are distinguished, namely, the single- and three-phase topologies. The first class has been widely treated in the literature, especially to equip photovoltaic systems such as described in [1]- [3]. The three-switch three-phase inverter (TSTPI), also known as B3 inverter or delta inverter (B3-VSI), has been firstly proposed by Evans et al. in the beginning of the 1980s [4]. The authors proposed a sinusoidal PWM (S-PWM) technique to control a B3-VSI fed IM drive. The resulting performances have been compared to that yielded by a B6 inverter [5]. In [6], Trzynadlowski et al. investigated the characteristics of the B3-VSI under the control of a dedicated SV- PWM technique considering the case of a RL-type load. As per the implementation of PWM methods in B3-VSI fed IM drives, and to the authors knowledge, no previous work dealing with this topic has been reported in the literature. In [7], they have proposed two SV-PWM methods based on the prediction of the conduction times of the involved power switches during each switching period considering different vector switching sequences.

This paper establishes and examines a comparative study between four CB-PWM dedicated for reduced structure B3 inverter fed induction motor drives. In the present work, another comparison study is carried out, considering four CB-PWM methods, namely: (i) S-PWM, (ii) third-harmonic injection PWM (THI-PWM), (iii) optimal PWM (OPT-PWM), and (iv) SV-PWM. The principle of operation of the B3-VSI fed IM drive is firstly presented with emphasis on the three-step operation mode. Then, a special attention is paid to the formulation of the power switch duty cycles and control sequences, and of the modulation functions. This enables the derivation of the modulation functions as well as of the fundamental voltage gains of the four CB-PWM methods. An experimentally-based comparison is treated within a case study, considering the open-loop operation of the B3-VSI fed IM drive. Prior to do so, the accuracy of the experimental setup is checked by simulation carried out in the Matlab-Simulink environment.

2. B3-VSI Fed IM Drives

a. Principle of Operation

The B3-VSI includes three power switches S_i and three freewheel diodes D_i, rather than six power switches and six freewheel diodes in conventional B6 inverter. This represents a crucial cost benefit for a large-scale production industry, such as the automotive one [8]. Each couple of S_i and D_i is mounted in series with a dc voltage source V_{dc}.

The three legs are delta-connected. The IM phase terminals are connected to the delta-summits, as illustrated in Fig. 1.

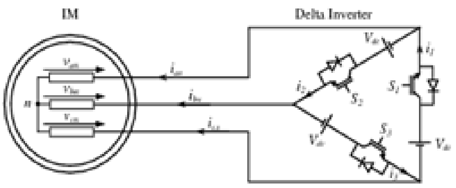

Fig. 1. Connections of the B3-VSI fed 3PIM drive.

The number of possible state combinations of the three power switches Si is 23 = 8. Nevertheless, the state combination ($S_1S_2S_3$) = (1 1 1), corresponding to ON-state of the three power switches ($\sum S_i = 3$), has to be discarded as far as it leads to a short-circuit of the three dc voltage sources. Considering the case of the IM (inductive load), the allowed combinations are reduced to three, corresponding to a simultaneous conduction of two power switches ($\sum S_i = 2$). In case of a star-connection of the IM stator phases, the line-to-neutral voltages van, vbn and vcn are expressed as:

$$\begin{bmatrix} v_{an} \\ v_{bn} \\ v_{cn} \end{bmatrix} = \begin{bmatrix} 1 & -1 & 0 \\ 0 & 1 & -1 \\ -1 & 0 & 1 \end{bmatrix} \begin{bmatrix} S_1 \\ S_2 \\ S_3 \end{bmatrix} V_{dc} \quad (1)$$

Tele: (+216 99 090 033
E-mail address: imn_nouira88@yahoo.fr

Table 1 summarizes the three possible state combinations, the corresponding stator phase voltages in a-b-c and α-β frames and the corresponding voltage vectors V_i. The voltage vectors V_i are located in the α-β frame as shown in Fig. 2.

Table 1. IGBTs states, phase voltages in a-b-c and α-β frames, and voltage vectors V_i.

$(S_1\ S_2\ S_3)$	v_{an}	v_{bn}	v_{cn}	v_α	v_β	V_i
(1 1 0)	0	V_{dc}	$-V_{dc}$	0	$\sqrt{2}V_{dc}$	V_1
(0 1 1)	$-V_{dc}$	0	V_{dc}	$-\sqrt{3/2}V_{dc}$	$-\sqrt{1/2}V_{dc}$	V_2
(1 0 1)	V_{dc}	$-V_{dc}$	0	$\sqrt{3/2}V_{dc}$	$-\sqrt{1/2}V_{dc}$	V_3

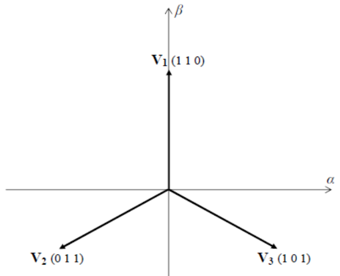

Fig. 2. Voltage vectors V_i of B3-VSI fed three-phase inductive load.

The line-to-line voltages are deduced by combining equation (1) and the relation $(\sum S_i = 2)$:

$$\begin{bmatrix} U_{ab} \\ U_{bc} \\ U_{ca} \end{bmatrix} = \left(2 - 3\begin{bmatrix} S_2 \\ S_3 \\ S_1 \end{bmatrix}\right) V_{dc} \tag{2}$$

Referring to equation (2), the line-to-line voltages have two unbalanced levels equal to $2V_{dc}$ and $-V_{dc}$.

a. Three-Step Operation Mode

Fig. 3 considers the three-step operation mode of B3-VSI characterized by the application of the control sequence "$V_3\ V_1\ V_2$" during two consecutive periods $2T_1$ of the fundamental component of the stator variables. It shows the waveforms of the phase voltages (v_{an}, v_{bn}, v_{cn}) and currents (i_{as}, i_{bs}, i_{cs}) as well as the line-to-line voltage Uab. From the analysis of the waveforms of the a-phase and the line-to-line voltages, their rms values are expressed as:

$$\begin{cases} v_{an(rms)} = \sqrt{\frac{2}{3}}V_{dc} \simeq 0.82V_{dc} \\ U_{ab(rms)} = \sqrt{2}V_{dc} \simeq 1.41V_{dc} \end{cases} \tag{3}$$

The instantaneous a-phase voltage v_{an} (t) is expressed in terms of Fourier expansion as:

$$V_{an}(t) = \frac{3V_{dc}}{\pi}\begin{bmatrix} \sin(w_1 t) - \frac{1}{2}\sin(2w_1 t) - \frac{1}{4}\sin(4w_1 t) \\ + \frac{1}{5}\sin(5w_1 t) + \frac{1}{7}\sin(7w_1 t) - \ldots \end{bmatrix} \tag{4}$$

Where: $w_1 = 2\pi f_1 = \frac{2\pi}{T_1}$

Similarly, the line-to-line voltage $U_{ab}(t)$ is expressed as a Fourier series:

$$U_{ab}(t) = \frac{3\sqrt{3}V_{dc}}{\pi}\begin{bmatrix} -\cos(w_1 t) + \frac{1}{2}\cos(2w_1 t) \\ -\frac{1}{4}\cos(4w_1 t) + \frac{1}{5}\cos(5w_1 t) \\ -\frac{1}{7}\cos(7w_1 t) - \ldots \end{bmatrix} \tag{5}$$

The *rms* values of the fundamental components are defined as follows:

$$\begin{cases} v^{(1)}_{an(rms)} = \frac{3V_{dc}}{\sqrt{2}\pi} \simeq 0.68V_{dc} \\ U^{(1)}_{ab(rms)} = \frac{3\sqrt{3}V_{dc}}{\sqrt{2}\pi} \simeq 1.17V_{dc} \end{cases} \tag{6}$$

Referring to equations (3) and (6), the total harmonic distortion THD_{l-n} of the line-to neutral voltage and the THD_{l-l} of the line-to-line voltage are equal, with:

$$THD_{l-n} = THD_{l-l} = \sqrt{\frac{4\pi^2}{27} - 1} \simeq 68\% \tag{7}$$

Compared to the voltage THD yielded by the B6 inverter under six-step operation mode, which is equal to $\sqrt{\frac{\pi^2}{9} - 1} \simeq 31\%$, one can notice that the THD of the voltages generated by the B3-VSI is almost 219% greater.

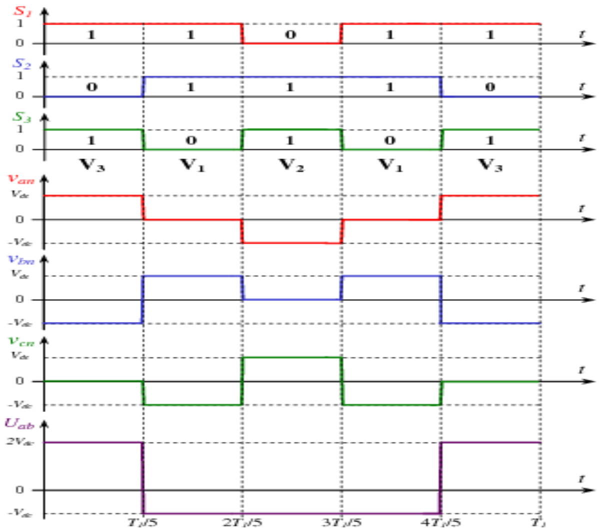

Fig. 3.Control signals, stator phase voltages (v_{an}, v_{bn}, v_{cn}), currents (i_{as}, i_{bs}, i_{cs}), and the line-to-line voltage U_{ab} under the three-step operation mode of the B3-VSI fed IM drive.

3. Carrier-Based Pulse Widht Modulation Methods

Basically, carrier-based PWM (CB-PWM) methods consist in a comparison of a carrier signal with a modulation one leading to the generation of the power switch control pattern. CB-PWM strategies are generally characterized by two operation modes, according to the peak value of the modulation signal is lower (linear modulation) or greater (overmodulation) than that of the carrier signal. In the case of B3-VSI, the three-step operation mode occurs at the end of the overmodulation mode.

a. Formulation of the Power Switch Duty Cycles

The modulation signals of the CB-PWM methods are the duty cycles dSi of the three power switches S_i. The derivation of their expression is developed hereunder.

Let us consider, for instance, the expression of the line-to-line voltage Uba which can be directly derived from equation (2), as:

$$U_{ba} = (3S_2 - 2)V_{dc} \tag{8}$$

The average value of Uba(av) is then expressed as follows:

$$U_{ba(av)} = (3d_{S2} - 2)V_{dc} \tag{9}$$

In the case of linear modulation, the reference value of $U_{ba(av)}$ noted U^*_{ba}, is expressed in terms of the modulation function F_{S2}, as:

$$U^*_{ba} = M\mathcal{F}_{S_2}(t)V_{dc} \tag{10}$$

Where M is the modulation index which is proportional to the ratio of the fundamental component rms value and to the dc voltage V_{dc}, with: $-1 \leq M\ F_{S2}\ (t) \leq 1$.

The equality between the average and reference values of U_{ba} yields:

$$d_{S_2}(t) = \frac{1}{3}\left[2 + M\mathcal{F}_{S_2}(t)\right] \tag{11}$$

A generalization of equation (11) leads to the following expression of the duty cycle dS_i :

$$d_{S_i}(t) = \frac{1}{3}\left[2 + M\mathcal{F}_{S_i}(t)\right] \tag{12}$$

Whose average value, during a fundamental period T_1 of the modulation signals, is calculated as:

$$d_{S_i(av)} = \frac{1}{T_1}\int_0^{T_1} d_{S_i}(t)dt = \frac{2}{3} \tag{13}$$

Equation (13) suggests that each power switch S_i is in ON-state during two-thirds of T_1 and in OFF-state during one-third of T_1.

a. Power Switch Control Sequences

Giving the fact that only two power switches Si of the B3-VSI could be in ON-state ($\sum S_i = 2$), the conventional CB-PWM methods dedicated to the B6 inverter control, based on a simple comparison of the three duty cycles d_{Si} and th carrier signal C_s, is no longer applicable. Consequently, a special attention has to be paid to the synthesis of the control sequences in the case of the B3-VSI. An approach to do so is developed hereafter.

Let us consider the case where the duty cycles fulfil the following inequalities:

$$d_{S_3} < d_{S_2} < d_{S_1} \tag{14}$$

and let us assume that they remain constant during a given number of the carrier signal periods, as illustrated in Fig. 4(a).

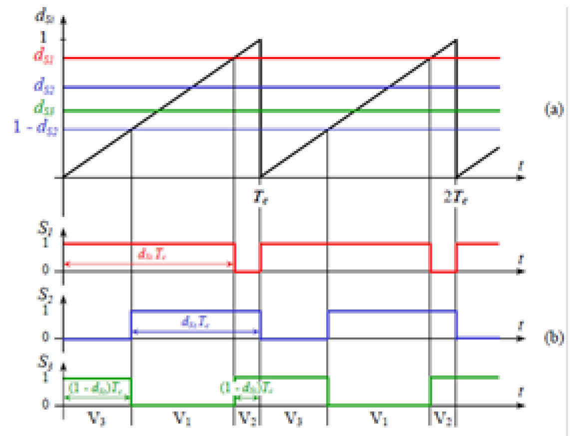

Fig. 4. Generation of the power switch control signals in the case where $d_{S3} < d_{S2} < d_{S1}$.

In order to satisfy the condition ($\sum S_i = 2$), the power switch control signals could be generated as following:

- the power switch S_1 is ON when $d_{S1} \geq C_s$,
- the power switch S_2 is ON when $1 - d_{S2} \leq C_s$,
- the power switch S_3 is ON when one among S_1 and S_2 is OFF.

The above-described approach has led to the power switch control signals shown in Fig.4(b), referring to which one can notice the following conduction times:

- the power switch S_1 is ON during $d_{S1}T_c$,
- the power switch S_2 is ON during $d_{S2}T_c$,
- the power switch S_3 is ON during $(1-d_{S1} + 1-d_{S2})T_c = (2-d_{S1}-d_{S2})T_c$.

Giving the fact that $\mathcal{F}_{Si}$ are balanced three-phase functions, equation (12) leads to:

$$\sum_{i=1}^{3} d_{S_i}(t) = 2 \tag{15}$$

Hence, and as desired, the conduction time of the power switch S_3 is equal to $d_{S3}T_c$.

a. Formulation of the Modulation Functions

A general expression of the modulation functions F_{Si} (t) can be written as:

$$\mathcal{F}_{S_i}(t) = k_F F_{S_i}(t) + E_0(t) \tag{16}$$

where k_F is the amplitude of the fundamental component of $F_{Si}(t)$, $E_0(t)$ is the zero-sequence signal, and $F_{Si}(t)$ are unity amplitude sinusoidal signals, such that:

$$\begin{cases} F_{S_1}(t) &= \sin(\omega_1 t) \\ F_{S_2}(t) &= \sin(\omega_1 t - \frac{2\pi}{3}) \\ F_{S_3}(t) &= \sin(\omega_1 t - \frac{4\pi}{3}) \end{cases} \tag{17}$$

In the manner of the B6 inverter, a characterization of the CB-PWM operation in the linear modulation range is achieved considering the fundamental voltage gain G_1. This latter is defined as the ratio of the fundamental component *rms* value $U^{(1)}_{[PWM]}$ of the line-to-line voltage to the fundamental component rms value $U^{(1)}_{[3\text{-Step}]}$ of the line-to-line voltage using the three-step operation mode (given by equation (6)), such as:

$$G_1 = \frac{U^{(1)}_{[\mathrm{PWM}]}}{U^{(1)}_{[3-\mathrm{Step}]}} = \frac{U^{(1)}_{[\mathrm{PWM}]}}{\frac{3\sqrt{3}V_{dc}}{\sqrt{2}\pi}} \simeq \frac{U^{(1)}_{[\mathrm{PWM}]}}{1.17V_{dc}} \tag{18}$$

Accounting for equations (2) and (12), the average value of the line-to-line voltages is expressed as:

$$U_{(av)} = M\mathcal{F}_{S_i}(t)V_{dc} \tag{19}$$

Equations (16) and (19) yield:

$$U^{(1)}_{[\mathrm{PWM}]} = M\frac{k_F}{\sqrt{2}}V_{dc} \tag{20}$$

4. Application to Different CB-PWM Methods

a. Sinusoidal PWM

The sinusoidal PWM (S-PWM) technique is characterized by pure sinusoidal modulation functions, which gives:

$$\begin{cases} k_F &= 1 \\ E_0(t) &= 0 \end{cases} \tag{21}$$

For S-PWM technique, the modulation functions $F_{Si}(t)$ are defined as:

$$\mathcal{F}_{S_i}(t) = k_F F_{S_i}(t) + E_0(t) = F_{S_i}(t) \tag{22}$$

The expression of the duty cycles d_{Si} turns to be as:

$$d_{S_i}(t) = \frac{1}{3}\left[2 + MF_{S_i}(t)\right] \tag{23}$$

Fig. 5(a1) shows the waveform of the fundamental component, the zero-sequence signal, and the resulting modulation functions $F_{S1}(t)$ in the case of a fundamental frequency f_1 = 50Hz. The corresponding duty cycle d_{S1} is shown in Fig. 5(b1) considering a unity modulation index.

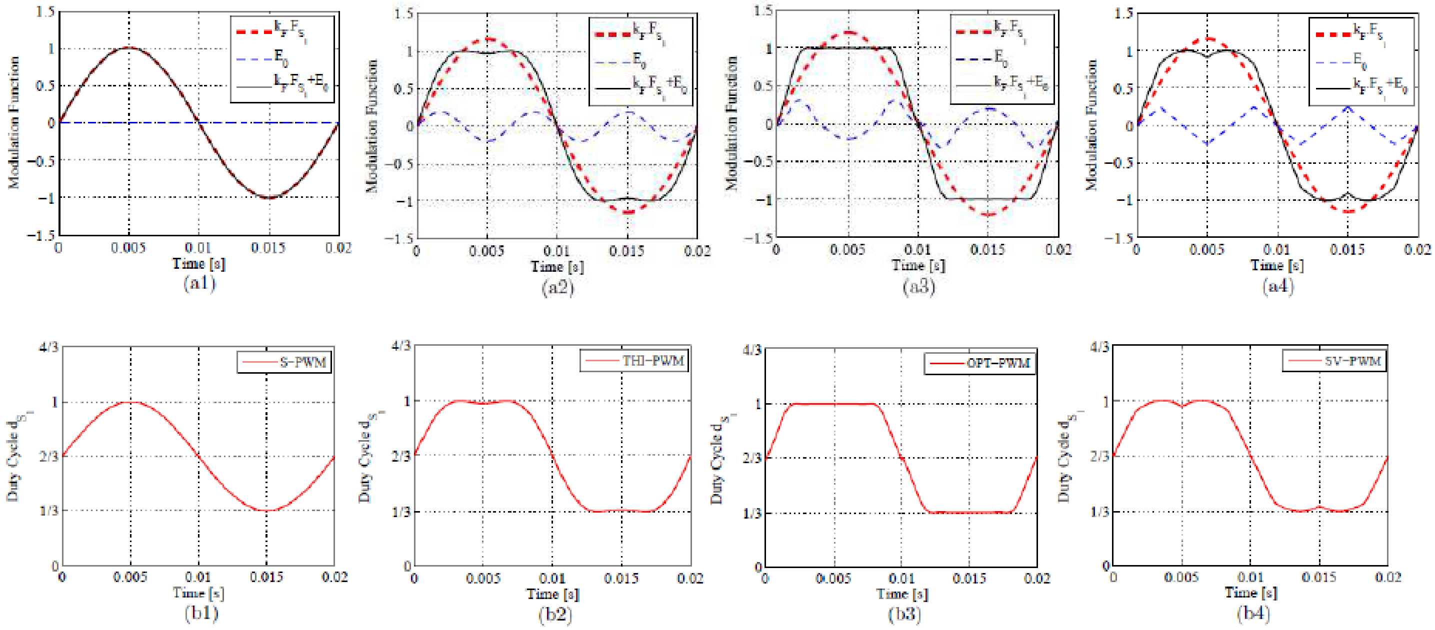

Fig. 5. Waveforms of (a) the modulation function and (b) the duty cycle of the power switch S_1 for f_1 = 50Hz and M = 1. Legend (1): S-PWM, (2): THI-PWM, (3): OPT-PWM, (4): SV-PWM.

Given the value of k_F = 1, the fundamental voltage gain is given by:

$$G_{1[\mathrm{S-PWM}]} = \frac{\pi}{3\sqrt{3}} M \simeq 0.605 M \qquad (24)$$

Therefore, the S-PWM is linear when the gain $G_{1[\mathrm{S-PWM}]}$ varies in the range [0% 60.5%]. Referring to [1] dealing with B6 inverters, the gain $G_{1[\mathrm{S-PWM}]}$ belongs to the interval [0% 78.5%].

a. Third-Harmonic Injection PWM

The third-harmonic injection PWM (THI-PWM) considers a zero sequence signal $E_0(t)$ which has an amplitude equal to the sixth of the fundamental one, as:

$$E_0(t) = \frac{k_F}{6} \sin(3\omega_1 t) \qquad (25)$$

The limit of the linear modulation range is achieved for $k_f = \frac{2}{\sqrt{3}} \approx 1.155$ which gives:

$$E_0(t) \simeq 0.193 \sin(3\omega_1 t) \qquad (26)$$

leading to the following expressions of the modulation functions $\mathcal{F}_{Si}(t)$ and of the duty cycles $d_{Si}(t)$:

$$\begin{cases} \mathcal{F}_{S_i}(t) = 1.155 F_{S_i}(t) + 0.193 \sin(3\omega_1 t) \\ d_{S_i}(t) = \frac{1}{3}\left[2 + M(1.155 F_{S_i}(t) + 0.193 \sin(3\omega_1 t))\right] \end{cases} \qquad (27)$$

Fig. 5(a2) gives the waveform of the fundamental component, the zero-sequence signal, and the resulting modulation functions $F_{S1}(t)$ in the case of a fundamental frequency f_1 = 50Hz. The corresponding duty cycle d_{S1} is shown in Fig. 5(b2) considering a unity modulation index.

Accounting for the value of $k_f = \frac{2}{\sqrt{3}}$, the fundamental voltage gain is expressed in terms of the modulation index as:

$$G_{1[\mathrm{THI-PWM}]} = \frac{2\pi}{9} M \simeq 0.7 M \qquad (28)$$

Hence, the THI-PWM is linear when the gain $G_{1[\mathrm{THI-PWM}]}$ varies in the range [0% 70%]. Referring to [1] dealing with B6 inverters, the gain $G_{1[\mathrm{THI-PWM}]}$ belongs to the interval [0% 90.7%].

a. Optimal PWM

The optimal PWM (OPT-PWM) technique consists in injecting the harmonics of ranks 3, 6, 9, and 12. It has been treated in the case of the B3-VSI in [9]. The proposed zero-sequence signal $E_0(t)$ is expressed as:

$$E_0(t) = \begin{bmatrix} 0.239\cos(3w_1 t) - 0.05\cos(6w_1 t) \\ -0.019\sin(9w_1 t) + 0.007\cos(12w_1 t) \end{bmatrix} \qquad (29)$$

The limit of the linear modulation range is achieved for k_F = 1.2, which enables the derivation of the expressions of $F_{Si}(t)$ and $d_{Si}(t)$ by applying equations (16) and (12), respectively.

Fig. 5(a3) gives the waveform of the fundamental component, the zero-sequence signal, and the resulting modulation functions $F_{S1}(t)$ in the case of a fundamental frequency f_1 = 50Hz. The corresponding duty cycle d_{S1} is shown in Fig. 5(b3) considering a unity modulation index.

Taking into consideration the value of k_F = 1.2, the fundamental voltage gain is expressed in terms of the modulation index as:

$$G_{1[\mathrm{OPT-PWM}]} = \frac{1.2\pi}{3\sqrt{3}} M \simeq 0.726 M$$

Consequently, the OPT-PWM is linear when the gain $G_{1[\mathrm{OPT-PWM}]}$ varies in the range [0% 72.6%]. Considering the case of B6 inverters, the gain $G_{1[\mathrm{OPT-PWM}]}$ belongs to a wider range, that is: [0% 94.2%].

a. Space Vector PWM

The CB-PWM technique inspired from the space vector PWM (SV-PWM) strategies has been commonly treated in the case of the B6 inverter [3], [4]. The considered zero sequence signal E0(t) is expressed as:

$$E_0(t) = -\frac{1}{2}\left[\max(F_{S_i}(t)) + \min(F_{S_i}(t))\right] \qquad (31)$$

The same zero-sequence signal has been considered in this work to the synthesis of a SV-PWM dedicated to B3-VSI. Giving the fact that the limit of the linear modulation range is achieved for $k_f \simeq 1.155$, the expressions of $F_{Si}(t)$ and $d_{Si}(t)$ could be derived applying equations (16) and (12), respectively.

Fig. 5(a4) gives the waveform of the fundamental component, the zero-sequence signal, and the resulting modulation functions $F_{S1}(t)$ in the case of a fundamental frequency f_1 = 50Hz.

The corresponding duty cycle dS1 is shown in Fig. 5(b4) considering a unity modulation index.

As far as the SV-PWM technique has the same value of k_f as the THI-PWM, the fundamental voltage gain $G_{1[SV-PWM]}$ has an expression similar to the one given in equation (28).

5. Case Study

This paragraph deals with the application of the above-developed CB-PWM methods to control a B3-VSI feeding an induction motor under open-loop operation.

For the sake of validation, the analytical results will be compared to those yielded by:

- simulation carried out in the Maltab-Simulink environment,
- experiments carried out on a developed test bench that will be described in the following paragraph.

a. Description of the Test Bench

In order to check the validity of the simulation program implemented in the Matlab Simulink environment, experimental tests have been carried out on a test bench including:

an induction machine which has the ratings and parameters given in Tables 2 and 3, respectively,

b. Simulation and Experimental Results

Table 2 . Induction mchine ratings.

Voltage	20 V /34 V	Speed	2830 rpm
Current	3 A / 1.73 A	Frequency	50 Hz

Table 3. Induction machine parameters.

$r_s = 0.8\ \Omega$	$l_s = 24$ mH	$M = 21.6$ mH	$J = 2e^{-4}$ kg.m^2
$r_r = 0.77\ \Omega$	$l_r = 24$ mH	$N_p = 1$	$f = 3e^{-4}$ N.m.s

- a B3-VSI made up of:
  - Six 12 V lead/acid batteries which are symmetrically-distributed on the three inverter-legs,
  - Three IGBT/Diode modules (using SKM 50 GB 123 D modules),
  - Three SKHI 22A modules are used as drivers for the IGBTs.
- A TMS320F240 DSP-based digital controller providing the IGBTs control signal and enabling the
- measurements of the stator phase voltages and currents.

A photograph of the experimental setup is presented in Fig. 6.

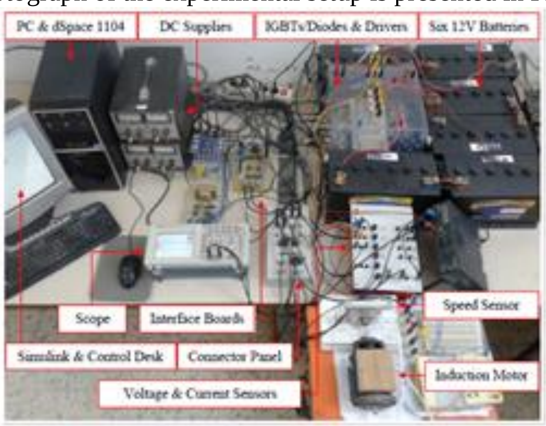

Figure 6. Photograph of the experiment platform for the B3-VSI fed IM drive.

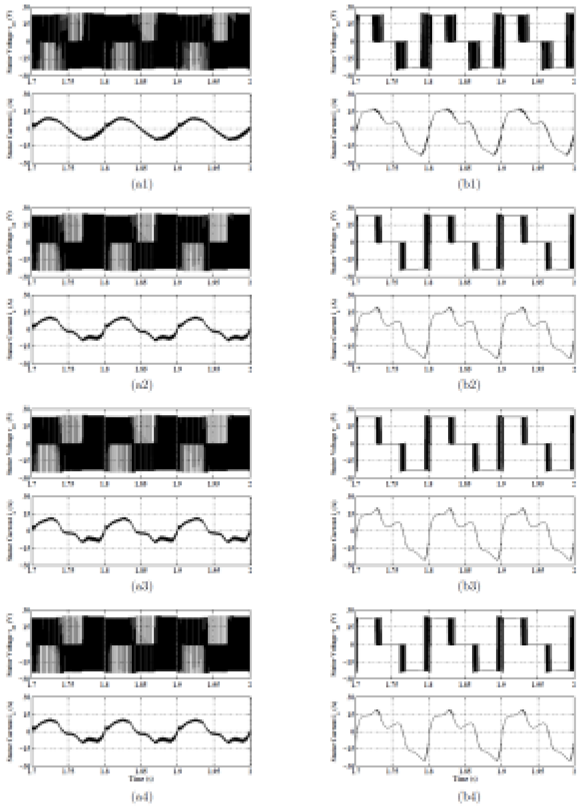

Figure 7 : Simulation results corresponding to the IM stator a-phase voltage van (top) and current i_a (bottom) for f_1 = 10 Hz. *Legend 1* (a): M = 1, (b): M = 3. Legend 2 (1): S-PWM, (2): THI-PWM, (3): OPT-PWM, (4): SV-PWM.

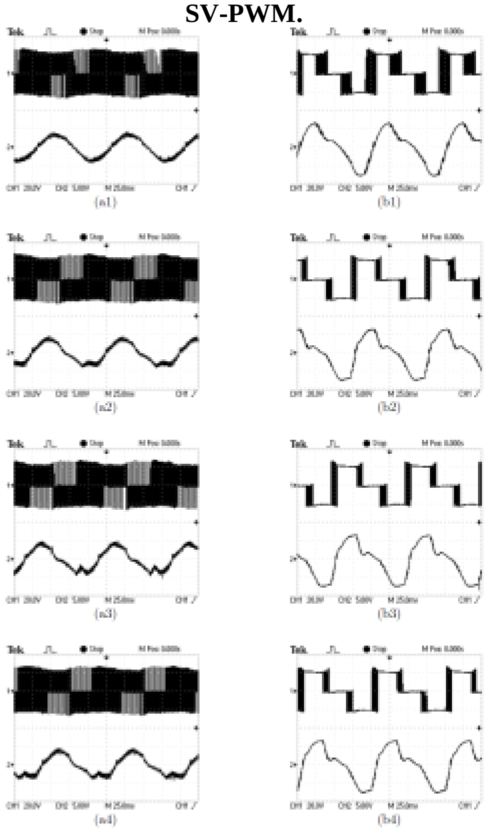

Figure 8: Experimental results corresponding to the IM stator a-phase voltage van (top) and current ia (bottom) for f1 = 10 Hz. Legend 1 (a): M = 1, (b): M = 3. *Legend 2* (1): S-PWM, (2): THI-PWM, (3): OPT-PWM, (4): SV-PWM.

The drive model has been implemented in the Matlab-Simulink environment assuming ideal dc-voltage sources in the B3-VSI legs. The IGBTs switching signals are generated by comparing the duty cycle signals dSi with a single-edge carrier signal. The carrier frequency fc is usually chosen greater than 20 times the fundamental frequency f_1 of the modulation signals. Both simulation and experiments consider a carrier frequency of 1kHz.

Fig. 7 shows the stator a-phase voltage and current waveforms obtained by simulation, for a fundamental frequency f_1 = 10Hz and for two values of the modulation index: M = 1 (subscripts “a”) which corresponds to the end of the linear modulation range, and M = 3 (subscripts “b”), considering the four CB-PWM strategies under study (subscripts (1): S-PWM, (2): THI-PWM, (3): OPT-PWM, and (4): SV-PWM).

Fig. 8 illustrates an experimental validation of the stator a-phase voltage and current waveforms shown in Fig. 7. One can notice a good agreement between simulation results and experimental measurements, with a maximum relative errors of the *rms* values of the phase voltage and current not exceeding 1% and 3%, respectively.

c.Analysis of the IM Current Harmonic Distortion

c1. Total Harmonic Distortion (THD)

This paragraph deals with an experimental investigation of the THD of the IM currents versus the modulation index M, covering linear modulation and overmodulation ranges, and considering three fundamental frequencies f_1 = 10, 30, and 50 Hz. The obtained results are shown in Fig. 9(1-3). One can notice that the THDs decrease with the increase of the modulation index M in the linear modulation range. Nevertheless, the harmonic distortion increases in the overmodulation range, leading to an increase of the THDs. The distortion characterizing the overmodulation range is more or less affecting the CB-PWM strategies under comparison. Indeed, the S-PWM technique yields the lowest harmonic distortion of the stator phase currents for all considered fundamental frequencies. The worst CB-PWM technique in terms of harmonic distortion is the OPT-PWM method.

Referring to Fig. 9(1), the THDs exhibited by the four CB-PWM strategies, considering the two operating points characterized by M = 1 and M = 3, are given in Table 4. These results are confirmed by the waveforms shown in Fig. 8.

Table 4. THD of the stator phase currents for f_1 = 10Hz and for M = 1 and M = 3.

THD	S-PWM	THI-PWM	OPT-PWM	SV-PWM
$M = 1$	11.3%	23%	27.2%	27%
$M = 3$	39.6%	45.5%	44.8%	45%

Now, let us focus the operating point characterized by f_1 = 50 Hz and M = 1 , as illustrated in Fig. 9(3). Experimental tests have been carried out and have led to the measurement of the stator a-phase current ias and the first-leg one i1, under the control of the four CB-PWM methods. The obtained results are shown in Fig. 10.

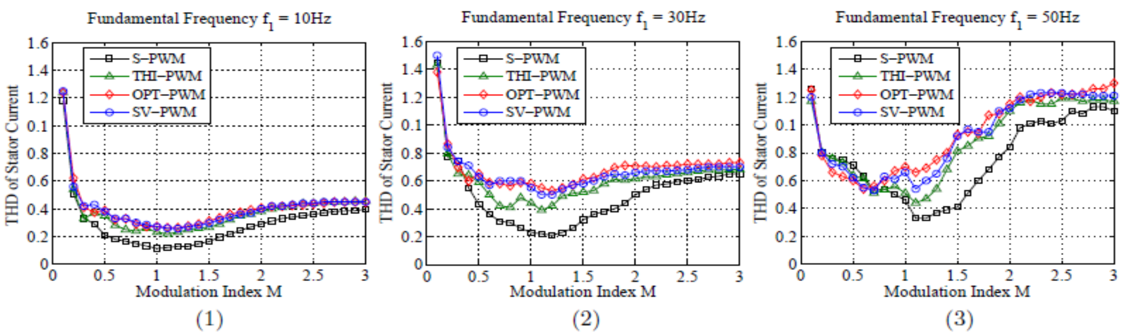

Figure 9. Experimental investigation of the variation of the IM stator current THD in terms of the modulation index M.

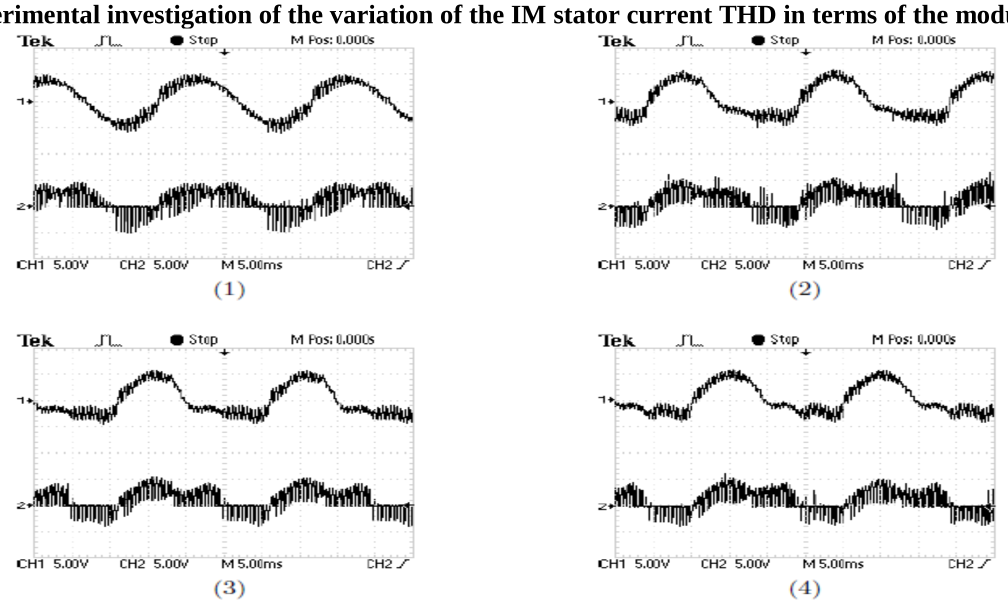

Figure 10. Scopes showing the experimental results corresponding to the steady-state operation of the B3-VSI fed IM drive under the control of the four CB-PWM methods for f1 = 50 Hz and M = 1. Legend 1 (top): stator a-phase current ias, (bottom) the first-leg current i1 (5 A/div). Legend 2 (1): S-PWM, (2): THI-PWM, (3): OPT-PWM, (4): SV-PWM.

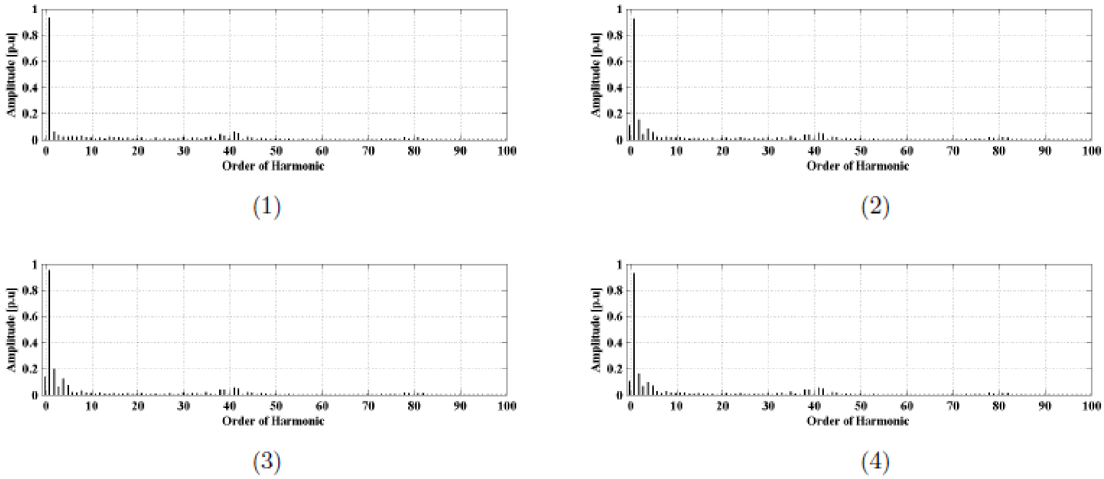

Figure 11. Spectra of the IM stator a-phase currents under the control of the four CB-PWM methods for f1 = 50 Hz and M = 1. Legend (1): S-PWM, (2): THI-PWM, (3): OPT-PWM, (4): SV-PWM.

Table 5. Amplitudes of the fundamental component and of the dominant low-order harmonics of the measured stator phase currents, as well as the corresponding PHDs, for f1 = 50 Hz and M = 1.

Harmonic Order	0	1	2	3	4	5	6	7	PHD[%]
S-PWM	0.11A	1.96A	0.15A	0.06A	0.06A	0.05A	0.04A	0.04A	11.11%
THI-PWM	0.29A	1.95A	0.56A	0.08A	0.22A	0.1A	0.03A	0.03A	34.94%
OPT-PWM	0.33A	1.96A	0.69A	0.1A	0.3A	0.11A	0.03A	0.03A	42.65%
SV-PWM	0.29A	1.96A	0.57A	0.12A	0.23A	0.12A	0.05A	0.03A	35.86%

Referring to Fig. 10, it is to be noted that, in spite of the quasi-sinusoidal waveform shown in Fig. 8(a1), the stator phase current yielded by the S-PWM technique turns to be distorted. This statement is confirmed by the increase of the THD of Fig. 9(3) with respect to the one of Fig. 9(1). A distortion level, slightly higher, is affecting the stator phase current yielded by the THI-PWM technique. However, the stator phase current waveforms yielded by the OPT-PWM and SV-PWM methods exhibit a higher distortion level than the S PWM one. Such a drawback is characterized by a 20% increase of THD, as illustrated in Fig. 9(3).

It comes out that the increase of the fundamental voltage gain achieved by the THI-PWM, OPT- PWM and SV-PWM methods is compromised by the increase of the harmonic distortion in the stator phase currents. An attempt to find out an interpretation of such a distortion is provided hereunder, considering an investigation of the partial harmonic content of the stator phase current.

c2. Partial Harmonic Distortion

Figs. 11(1-4) give the spectra of the stator a-phase currents yielded by simulation. These results clearly show that the major differences between the four spectra are due to low-order harmonics. In order to characterize the significance of the dominant harmonics, a partial harmonic distortion (PHD) ratio is defined as:

$$\mathrm{PHD} = \frac{1}{I_1}\sqrt{\sum_{n\neq 1} I_n^2}$$

where n is the order of the selected harmonic component.

Table 5 provides the amplitudes of the fundamental component and of the dominant low-order harmonics (ranks n = 0, 2, 3, 4, 5, 6, and 7) of the measured stator phase currents shown in Fig. 11, as well as the corresponding PHDs, yielded by the four CB-PWM methods. From the analysis of the results given in Table 5, the following remarks could be distinguished:

- the amplitudes of the fundamental components are almost equal,
- the amplitudes of the harmonics of ranks 0, 2, and 4 are significantly higher under the THI-PWM, OPT-PWM and SV-PWM methods than those yielded by the S-PWM one,
- the PHDs of the dominant low-order harmonics yielded by the THI-PWM, OPT-PWM, and SV-PWM methods are respectively 3.1, 3.8, and 3.2 greater than that of the S-PWM one.

5. Conclusion

This paper dealt with a comparison between the performance of four carrier-based pulsewidth modulation (CB-PWM) methods dedicated to B3-VSI fed induction motor (IM) drives, namely: (i) sinusoidal PWM (S-PWM), (ii) third-harmonic injection PWM (THI-PWM), (iii) optimal PWM (OPT-PWM), and (iv) space-vector PWM (SV PWM). The study has been initiated by the basis of the B3-VSI fed IM drive with emphasis on the three-step operation mode. Then, a special attention has been paid to the derivation of a general formulation of (i) the power switch duty cycles and control sequences, and (ii) the modulation functions allied to the fundamental voltage gain. The established expressions have been adapted considering each of the CB-PWM methods under comparison.

The comparison between the four CB-PWM methods has been achieved by an investigation of the THDs of the IM stator phase current. It has been shown that the THDs decrease with the increase of the modulation index in the linear modulation range. Nevertheless, the overmodulation range is characterized by an increase of the THDs with the modulation index, more or less significant according to the CB-PWM technique. Indeed, the S-PWM yields the lowest harmonic distortion of the stator phase currents for all considered fundamental frequencies. The worst CB-PWM technique in terms of harmonic distortion is the OPT-PWM.

In light of the achieved comparative study, it has been clearly demonstrated that the S PWM technique is the most suitable in controlling a B3-VSI feeding an IM. This statement is not applicable in the case of the B6 inverter fed IM drive for which it is well known that the THI-PWM and SV-PWM methods lead to the best performance.

References

[1] M. Hava, R. J. Kerkman, and T. A. Lipo, “A high-performance generalized discontinuous PWM algorithm,” IEEE Trans. Ind. Appl., vol. 34, no. 5, pp. 1059-1071, 1998.

[2] Y. Sun, Y. Liu, M. Su, W. Xiong, and J. Yang, “Review of active power decoupling topologies in single-phase systems,” IEEE Trans. Power Electron., vol. 31, no. 7, pp. 4778-4794, 2015.

[3] M. H. Zare, M. Mohamadian, and R. Beiranvand, “A single-phase grid-connected photovoltaic inverter based on a three-switch three-port flyback with series power decoupling circuit,” IEEE Trans. Ind. Electron., vol. 64, no. 3, pp. 2062-2071, 2017.

[4] P. D. Evans, R. C. Dodson, and J. F. Eastham, “Delta Inverter,” IEE Proc., vol. 127, no. 6, pp. 333-340, 1980.

[5] P. D. Evans, R. C. Dodson, and J. F. Eastham, “Sinusoidal pulsewidth modulation strategy for delta inverter,” IEEE Trans. Ind. Appl., vol. IA-20, no. 3, pp. 651-655, 1984.

[6] A. M. Trzynadlowski, and S. Legowskis, “Characteristics of the delta inverter with vector pulse width modulation,” Int. J. Electronics, vol. 76, no. 6, pp. 1205-1219, 1994.

[7] I. N. El Badsi, B. El Badsi, and A. Masmoudi, “Space vector PWM methods for B3-VSI fed three-phase IM drives,” IEEE Vehicle Power and Propulsion Conference (VPPC), 17-20 Oct., pp. 1-6, 2016.

[8] A. M. El-Antably, A. Ben Rhouma, A. Masmoudi, and A. G. Holmes, “Control device for driving a brushless DC motor,” US 7643733 B2, 2010.

[9] A. M. Trzynadlowski, S. Ji, and S. Legowski, “Random pulse width modulation of delta inverter for automotive applications,” in Proc. Conf. Rec. 1991 IEEE-IAS Ann. Mtg, pp. 826-833, 1991.